COMMUNICATION

Reversible High-Capacity Si Nanocomposite Anodes for Lithium-ion Batteries Enabled by Molecular Layer Deposition

Daniela Molina Piper, Jonathan J. Travis, Matthias Young, Seoung-Bum Son, Seul Cham Kim, Kyu Hwan Oh, Steven M. George, Chunmei Ban, and Se-Hee Lee**

The development of high-energy lithium-ion batteries (LIBs) requires the incorporation of high-capacity materials, such as silicon, to replace the currently commercialized graphite anode.[1,2] Si has become one of the most highly investigated materials for LIB anodes because of its ability to accommodate 3.75 moles of Li per mole of Si ($Li_{15}Si_4$) for a theoretical capacity of 3579 mA h g^{-1} at room temperature, as compared with 372 mA h g^{-1} for graphite (1 mol Li per 6 mol C).[3,4] Despite Si's inherent advantages, progress towards a commercially viable Si anode has been impeded by Si's rapid capacity fade, poor rate capability, and low coulombic efficiency (CE).

Si exhibits volume changes of ~300% upon lithium alloying and de-alloying, leading to material degradation and presenting a major problem for electrochemical performance. Even though pulverization of the Si particles themselves due to volume changes can be mitigated by integrating particles smaller than 150 nm,[5] the cracking and breaking of the electrode composite, and thereby its conductive network, have become the biggest challenge impeding the realization of a Si-based anode. This high volume expansion and contraction is too large to be controlled by currently developed coating technologies, including the use of surface modifications such as atomic layer deposition (ALD) of metal-oxide (MO)[6] and carbon coatings.[7] As the electrode matrix fractures, the continuous exposure of fresh nano-Si surface to the liquid electrolyte causes parasitic formation of a solid-electrolyte interphase (SEI) leading to irreversible charge loss and low CE. Fractures also incite particle agglomeration and isolation, which contribute to further cell degradation.[1,8,9] Protection of the nano-Si particles from reactions with the liquid electrolyte, from agglomeration, and from isolation is essential throughout cycling. Developing an effective electrode matrix that is capable of accommodating massive volumetric changes and protecting the electrode surface throughout the battery's cycle life is critical to the mitigation of many issues that have impeded the commercialization of nano-Si-based anodes.

Much effort has been devoted to the development of integrated Si matrices and coatings prior to the manufacturing of the electrodes.[10–13] Two main front-end strategies have been established for the realization of such an approach: 1) embedding nano-Si particles in hard-confinement host matrices in order to attempt to buffer the volume expansion of the particles,[10–12] and 2) coating nano-Si particles with flexible materials in order to attempt to accommodate the volumetric changes of the particles.[13] Even though previous reports involving hard-confinement host matrices have shown to be promising, the host matrices are brittle and have a tendency to fail upon continuous expansion and contraction.[9,14] On the other hand, previous reports by our group and others on flexible coatings for Si-based electrodes have shown that electrode binders with elastic properties lead to remarkably improved cycling stability.[13] These previous studies have proven that elastic, flexible coatings that can accommodate severe volume changes, are necessary for the stabilization of high-capacity Si anodes.

The aforementioned work focused on solving the issues associated with Si cycling behavior on the front-end of the electrode fabrication procedure, integrating binder matrices and powder coatings prior to the manufacturing of the electrodes. In contrast, work on the back-end of the electrode fabrication process has been limited to surface modification of manufactured electrodes with MOs via ALD. While recent work has proven ALD to be an important tool in improving the performance of LIB electrodes via surface coating,[15] attempts to attenuate volume expansion in high-capacity electrodes have been unsuccessful. ALD-MO coatings may help reduce the effect of parasitic side reactions between the liquid electrolyte and electrode surface, but the coatings are not robust enough to provide structural support when applied to materials such as Si, which undergo volumetric expansion of up to 300%.

In order to address the challenge of Si's dramatic volumetric change, we carried out a surface modification, in which molecular layer deposition (MLD) was utilized to grow a mechanically robust, flexible coating, producing high-capacity Si nanocomposite anodes. Techniques based on ALD allow for the growth

D. Molina Piper, Prof. S. M. George, Prof. S.-H. Lee
Department of Mechanical Engineering
University of Colorado at Boulder
Boulder, CO, 80309, USA
E-mail: sehee.lee@colorado.edu
J. J. Travis, Prof. S. M. George
Department of Chemistry and Biochemistry
University of Colorado at Boulder
Boulder, CO, 80309, USA
M. Young
Department of Chemical Engineering
University of Colorado at Boulder
Boulder, CO, 80309, USA
D. Molina Piper, Dr. C. Ban
National Renewable Energy Laboratory
1617 Cole Boulevard,
Golden, CO, 80401, USA
E-mail: Chunmei.Ban@nrel.gov
S.-B. Son, S. C. Kim, Prof. K. H. Oh
Department of Material Science and Engineering
Seoul National University
Seoul, 151-742, Korea

DOI: 10.1002/adma.201304714

of conformal thin films of inorganic materials using sequential, self-limiting reactions. The films are conformal, meaning that they can penetrate and coat high-surface area tortuous structures thoroughly. MLD methods extend this strategy to include organic and hybrid organic–inorganic polymeric materials.[16] The thin, conformal, and flexible MLD coating is able to penetrate the electrode's porous structure and covalently bind to available surfaces. This creates a strong, flexible network within the electrode that binds the materials and ensures sufficient contact area throughout cycling. By coating nano-Si composite anode electrodes with polymeric aluminum glycerol (AlGL) via MLD,[17] we show that it is possible to cycle nano-Si composite electrodes for over 100 cycles with capacities of nearly 900 mA h g^{-1} and CEs in excess of 99%.

In this work, AlGL was deposited conformally onto Si anodes using the sequential, self-limiting reaction of trimethylaluminum ($Al(CH_3)_3$) and glycerol ($C_3H_5(OH)_3$) according to:

A. Reaction A: $R–OH^* + Al(CH_3)_3 \rightarrow R–O–Al(CH_3)_2^* + CH_4$

B. Reaction B: $R–O–Al(CH_3)^* + C_3H_5(OH)_3 \rightarrow R–O–Al–OC_3H_5(OH)_2^* + CH_4$

where asterisks indicate surface species and R represents the underlying Si electrode. The resulting poly(aluminum glycerol) is also referred to as alucone, and is part of a broader new class of materials referred to as metalcones.[18,19] **Figure 1** shows a schematic of the controlled layered chemistry structure of the AlGL used in this work. The growth rate of this MLD reaction is known to be 2.5 Å per AB cycle at a substrate temperature of 140 °C.[17] Due to the presence of more than two hydroxyl groups per glycerol molecule, sequential reactions between ($Al(CH_3)_3$) and ($C_3H_5(OH)_3$) produce a high degree of cross-linking between the polymer chains, which strengthens the alucone films and lead to higher fracture toughness.[19] This added fracture toughness is ideal for accommodating the massive volumetric changes of the nano-Si composite electrode.

Transmission electron microscopy (TEM) and electron energy loss spectroscopy (EELS) were utilized to characterize the microstructure of the nano-Si/AlGL electrodes. TEM samples were prepared using a focused ion beam (FIB) equipped with a mobile air-lock chamber.[10] Images of the TEM sample preparation are presented in the Supporting Information (SI; Figure S1). **Figure 2** presents TEM images (Figure 2a,c) and an EELS elemental map (Figure 2d) of an uncycled nano-Si/AlGL electrode. We observe a conformal thin coating of AlGL (red mapping) on the nano-Si particles (cyan mapping). High-angle annular dark-field (HAADF) scanning transmission electron microscopy (STEM), which is highly sensitive to atomic-number contrast (Z-contrast imaging), was used to further clarify the conformity of the AlGL coating on the nano-Si particles. Through HAADF-STEM (Figure 2b), we prove that the AlGL layer is a thin (~5 nm), dense, and conformal coating adhering to the nano-Si particles. This conformal coating of the highly porous composite electrodes (Figure 2a) was achieved using static dosing of the AlGL precursors.[19]

Electrochemical characterization was utilized to study the AlGL coating's ability to improve Si electrode cycling performance. Figure 2e presents the cyclic stability of the nano-Si/AlGL anode against the stability of the nano-Si/bare composite electrode. The nano-Si/AlGL electrode was run at a rate of *C*/20 for the first 10 cycles and a rate of *C*/10 for all subsequent cycles, where *C* is the *C*-rate, the rate equivalent to a full charge/discharge of the electrode in 1 h. The bare nano-Si electrode was run at *C*/20 throughout its short cycle life. At cycle 150, the nano-Si/AlGL cell exhibits a specific charge capacity of nearly 900 mA h g^{-1} with a CE in excess of 99%, whereas the nano-Si/bare electrode undergoes rapid degradation of a typical Si-based composite electrode, failing by its 30th cycle. The specific charge capacity of 900 mA h g^{-1} of the nano-Si/AlGL corresponds to an electrode volumetric capacity of 569 mA h cm^{-3} considering an initial electrode thickness of 12.74 µm (**Figure 3**d). Such good cycle life and CE are evidence that the AlGL electrode coating provides favorable mechanical properties, accommodating the volumetric changes of the nano-Si particles and preserving the structural integrity of the electrode network throughout cycling.

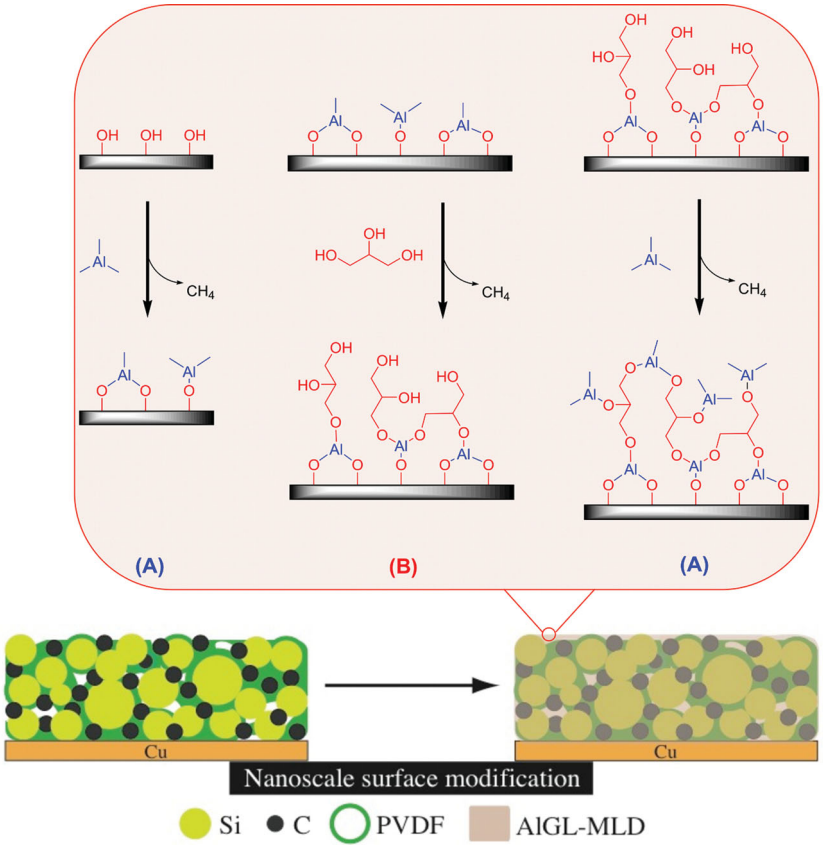

Figure 1. Schematic of the controlled layered chemistry structure of the AlGL used to coat the conventional Si nanocomposite electrodes. The AlGL coating is based on sequential, self-limiting reactions of trimethylaluminum ($Al(CH_3)_3$) and glycerol ($C_3H_5(OH)_3$). The growth rate of this MLD reaction is known to be 2.5 Å per AB cycle at a substrate temperature of 140 °C. PVDF represent the binder, polyvinylidene fluoride.

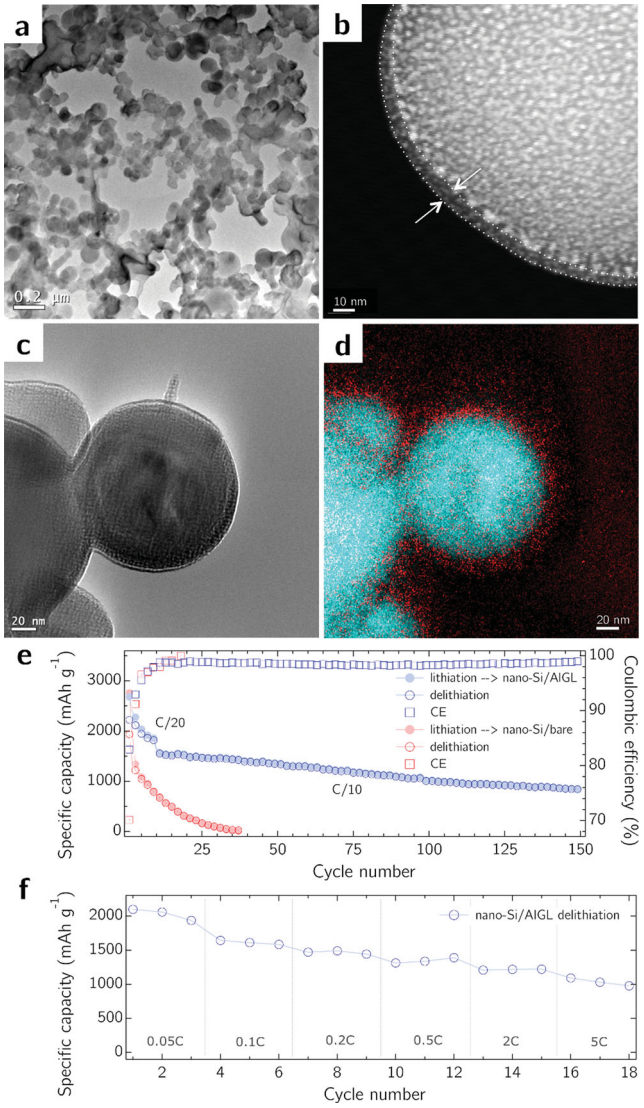

Figure 2. a) TEM image of an uncycled nano-Si/AlGL electrode showing a highly porous composite network. b) HAADF-STEM image of an uncycled nano-Si particle coated with AlGL. The high sensitivity to atomic number of HAADF-STEM shows a thin (~5 nm), dense, and conformal coating of AlGL adhered to the nano-Si particle highlighted by the white arrows and dotted lines. c) TEM image of the uncycled nano-Si/AlGL electrode with d) EELS elemental mapping (Si: cyan; Al: red) confirming that a conformal AlGL coating is achieved throughout the Si nanocomposite. e) Cyclic capacity and CE (blue symbols) of a nano-Si/AlGL anode in comparison with the capacity and CE (red symbols) of a nano-Si/bare composite electrode. At cycle 150, the nano-Si/AlGL cell shows a specific charge capacity of nearly 900 mA h g^{-1} with a CE in excess of 99%, whereas the nano-Si/bare electrode fails after 30 cycles. f) A rate test demonstrates that the nano-Si/AlGL electrode can achieve an average specific charge capacity of 1033 mA h g^{-1}.

The first cycle CE of 83% is evidence of an improved interface between the electrode and liquid electrolyte, suggesting that the MLD coating layer passivates irreversible charge loss due to unwanted side reactions. To confirm the possible passivating properties of the AlGL coating, we first looked at the voltage profile of the initial lithiation cycle of both the nano-Si/AlGL electrode and that of the nano-Si/bare electrode (SI: Figure S2). The irreversible capacity observed at 0.6 V during initial lithiation is pronounced only on the bare electrode and is ascribed to the reduction of the liquid electrolyte and the formation of the SEI layer.[20] The AlGL coating therefore helps mitigate the secondary reactions that happen between the liquid electrolyte and the electrode surface. To further substantiate the passivating properties of the AlGL coating, we analyzed its stability against the liquid electrolyte for hundreds of cycles and with a wider voltage range of 0.05–2 V (SI: Figure S2). We coated half-inch stainless-steel spacers with 5 cycles of AlGL and tested in a half-cell configuration with charging and discharging currents of 1.5 µA. The results show an excellent stability of the coating against the liquid electrolyte for a long cycling progression. The AlGL coating exhibits good passivating properties and long cycle life stability against the liquid electrolyte, helping to mitigate the parasitic formation of an SEI with exposed fresh nano-Si surfaces not only during the initial cycles of formation but throughout the cells' cycle life.

In lieu of a direct electrical conductivity measurement of the AlGL electrode coating, we used electrochemical impedance spectroscopy (EIS) to measure ohmic resistance. The ohmic resistance of the nano-Si/bare electrode was found to be 2.67 Ω, whereas that of the nano-Si/AlGL anode was 3.18 Ω. Thus, the contribution to the total ohmic resistance by the AlGL coating was only 0.51 Ω (SI: Figure S3). We also conducted a rate test to study the transport properties of the AlGL coating (Figure 2f). At a rate of 5*C*, the nano-Si/AlGL electrode exhibited an average specific charge capacity of 1033 mA h g^{-1}. If the AlGL coating did not provide adequate ionic and electronic transport, it is reasonable to conclude that we would not have been able to achieve such high charging capacities at a rate of 5*C*. At this time, a direct ionic and electronic transport mechanism for the AlGL coatings has yet to be elucidated.

In order to study the resilience of the nano-Si/AlGL MLD electrode microstructure to the effects of Si volumetric expansion, scanning electron microscopy (SEM) samples were prepared from electrodes at different stages of cycle life. Figure 3 presents SEM images of electrode cross-sections before and after initial lithiation and then after the 20th delithiation cycle of both the bare and AlGL-coated electrodes. Figure 3a and d show the cross-sections of the uncycled bare and AlGL-coated electrodes with an initial thickness of 12.15 and 12.74 µm, respectively. The discrepancy in initial thickness between the bare electrode and the coated electrode is because of the variance introduced in the manufacturing of the electrodes. Figure 3b and e present the initial lithiation of the bare and coated electrode, respectively. The volume expansion during the initial lithiation of both the bare and the AlGL-coated electrode lies around 70–80%. Si's expansion is largely accommodated by the porosity of the electrode in both coated and uncoated anodes. While the AlGL coating does not prevent Si from free volume expansion during complete lithiation,[12] it does allow for a nearly full recovery from the massive volumetric expansion upon delithiation after 20 cycles. The AlGL coating helps preserve the electrode network, which is highlighted by the observed 17.5% volume increase after 20 electrochemical cycles (Figure 3f) as compared to the 50% volume increase of the bare electrode (Figure 3c). The bare electrode loses

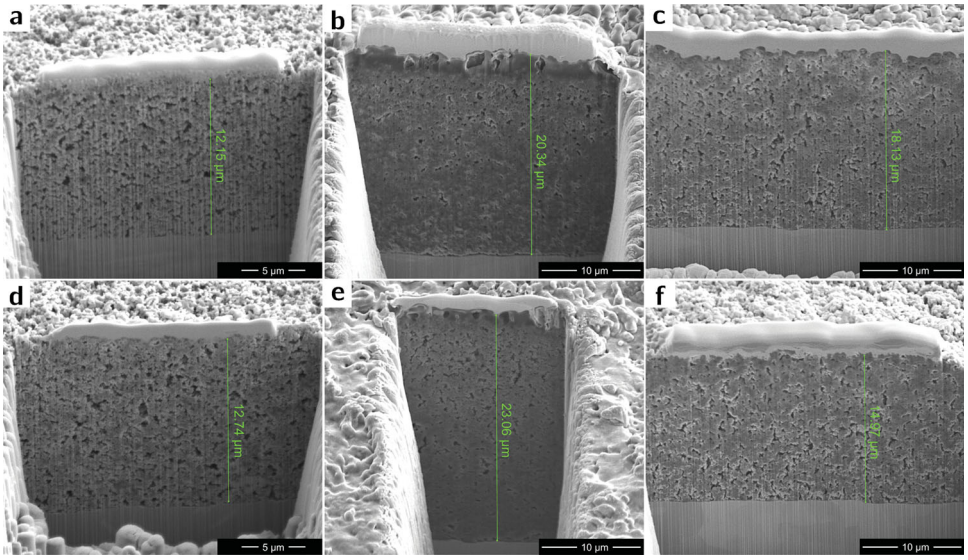

Figure 3. SEM images of electrode cross-sections a,d) before and b,e) after initial lithiation and then c,f) after the 20th delithiation cycle for the bare (a–c) and AlGL-coated (d–f) electrodes. At initial lithiation of the bare and coated electrode, the volume expansion lies around 70–80%. Si's expansion is largely accommodated by the porosity of the electrode in both coated and uncoated anodes. Upon delithiation after 20 cycles, the bare electrode's network remains almost fully expanded losing fundamental particle contact and structural integrity, whereas the AlGL coating helps preserve the electrode network, which is highlighted by the observed 17.5% volume increase after 20 electrochemical cycles.

fundamental particle contact and structural integrity, resulting in rapid degradation. It is concluded that the AlGL coating provides sufficient mechanical support to both accommodate the major volumetric changes experienced by the Si nanocomposite anodes and to aid in the recovery and preservation of the whole composite network upon delithiation.

To prove that the AlGL coating conforms to the strains of lithiated Si and aids in the recovery and preservation of the electrode upon delithiation, more in-depth TEM images of the electrodes' cross-sections were analyzed. **Figure 4** presents the TEM images of the nano-Si/bare electrode (Figure 4a,b) and the nano-Si/AlGL electrode (Figure 4d,e). The bare electrode shows a severance of the connections between the nano-Si particles and the electrode network once delithiation occurs, and the particles contract (see Figure 4c for a detailed schematic of this separation mechanism). This behavior isolates active material and prevents its utilization, thus contributing to rapid capacity degradation. On the other hand, the AlGL-coated electrode shows an intimate adherence between the Si nano-particles and the rest of the electrode network (Figure 4e) during initial cycling. This intimate contact between particle and coating provides a linked conductive network that prevents the isolation of active material and enables its full utilization throughout cycling (SI: Figure S4).

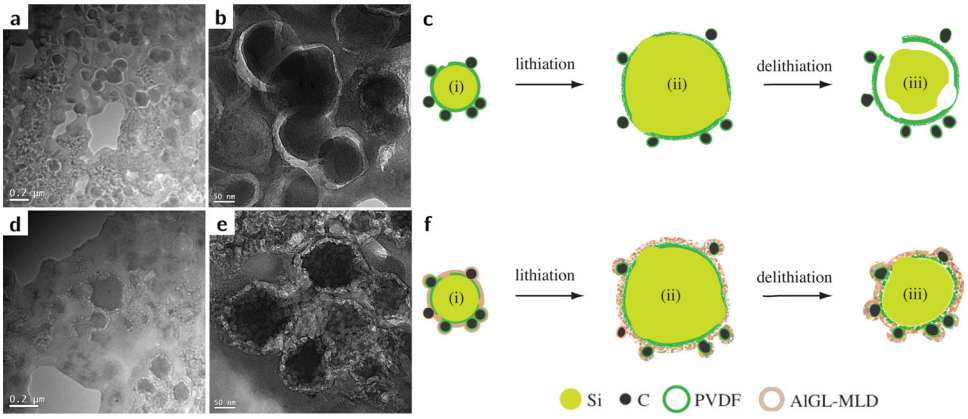

Figure 4. a,b) TEM images of the nano-Si/bare electrode. The bare electrode shows a severance of the connections between the nano-Si particles and the electrode network once delithiation occurs and the particles contract. This behavior isolates active material and prevents its utilization. c) Detailed schematic of the nano-Si/bare electrode's lithiation–delithiation mechanism. d,e) TEM images of the nano-Si/AlGL-coated electrode. The AlGL-coated electrode shows an intimate adherence between the Si nano-particles and the rest of the electrode network. This particle/coating intimacy provides a linked conductive network that prevents the isolation of active material and enables its full utilization throughout cycling. f) Detailed schematic of the nano-Si/AlGL electrode's lithiation–delithiation mechanism. PVDF represent the binder, polyvinylidene fluoride.

We believe the coating maintains covalent contact with the nano-Si particles during expansion upon lithiation, Figure 4f(i)–(ii), accommodating the large volume changes. Because the coating is covalently bound to both the particles and the electrode network, it aids in recovering the electrode network to its initial state, retaining intimate contact with the nano-Si particles upon delithiation, Figure 4f(ii)–(iii). The particle and coating surface roughness observed is attributed to the anisotropic expansion of the Si nanoparticles.[21] Further characterization is needed to explain the exact mechanism of improved cycling stability in the coated Si nanocomposite electrodes, and future work will focus on this. While the average particle size of the active material is under the critical size for crack formation and propagation,[5] it is likely that there is some exposed active-material surface that reacts with the liquid electrolyte and leads to the slight degradation seen throughout cycling. Given the observed electrochemical and spectroscopic data, it is concluded that an AlGL coating maintains a mechanically robust, resilient, and highly conductive network for the Si composite electrodes, allowing for a long cycle life and remarkable stability.

The application of AlGL conformal coatings as a surface modifier for high-capacity electrodes represents a novel advancement in electrochemical applications. Surface modification work has previously been limited to ALD-MO, which is not suitable for materials with large volume changes due to mechanical failure under large stresses. AlGL is a solution to many of the ongoing issues that have hindered the commercialization of Si nanoparticles and other high-capacity anode materials. The employment of AlGL on conventional nano-Si composite electrodes provides significant improvement in cycling stability, rate, and CE. We show that the AlGL coating is highly stable against liquid electrolyte and acts as a passivating agent to protect the active material from unwanted secondary reactions. AlGL also proves to be robust and resilient enough to accommodate the extreme volumetric changes of the Si nanocomposite electrodes, helping to maintain an intimately linked conductive network and allowing for faster ionic and electronic conduction. This favorable combination of mechanical and electrochemical properties allows the AlGL surface modification to greatly enhance the performance of nano-Si electrodes. As the described electrode fabrication process is compatible with commercial electrode manufacturing methods, this research may be adaptable to many other high-capacity materials and introduces a potentially major advancement in LIB technology.

Experimental Section

Molecular Layer Deposition: AlGL films were grown directly on the nano-Si composite electrodes using a pancake reactor (see main text and Figure 1 for detailed chemistry). The typical growth rate for AlGL chemistry is 2.5 Å per cycle. The AlGL reaction sequence was the following: i) dose trimethylaluminum for 2 s; ii) hold trimethylaluminum pressure static for 90 s; iii) flow purge for 180 s; iv) 5 cycles of argon static purge; v) dose glycerol for 2 s; vi) hold glycerol pressure static for 120 s; vii) flow purge for 240 s; and viii) 7 cycles of argon static purge. Flow purge was performed by pumping out excess precursors and reaction by-products while flowing argon through the reactor. Argon static purge was performed by dosing argon for 20 s, holding the argon pressure static for 5 s, evacuating for 45 s, and flow purging for 20 s. This sequence constitutes of one AB cycle of AlGL. The electrodes were coated with 21 cycles of AlGL, and the reaction was conducted at 140 °C. The effect of the MLD coating thickness on the nano-Si composite anodes had been investigated (SI: Figure S5), and 21 cycles of AlGL was selected based on its optimal performance.

Material Preparation: The nano-Si-based composite electrodes were prepared by spreading nano-Si powder (50 nm, Alpha Aesar), acetylene black, and PVDF (polyvinylidene fluoride, binder) mixed in *N*-methyl pyrolidinone solvent (60:20:20 weight ratio) on a piece of Cu foil. Once the electrodes were dried and calendared, some were treated with AlGL coating. Before assembling the cells, the half-inch (1 inch = 2.54 cm) punched electrodes were dried overnight (120 °C) in a vacuum oven. Cells were assembled in an Ar-dry box and tested at room temperature. Electrochemical measurements were normalized based on the mass of the nano-Si in each electrode (typically 0.8–1.0 mg).

Electrochemical Measurements: Electrochemical measurements were carried out using an Arbin 2000 battery test station. All cells were assembled in an Ar-filled glove-box using the prepared nano-Si/bare or nano-Si/AlGL electrodes as the working electrodes and lithium metal foil as the counter-electrode. The electrolyte was 1 m $LiPF_6$ dissolved in a 1:1 (volume ratio) mixture of ethylene carbonate (EC) and diethyl carbonate (DEC); the separator was a glass micro-fiber disk (Whatman GF/F), and the shell was a stainless steel CR2032 coin cell (VWR Inter.). We used a (constant current)–(constant voltage) (CCCV) testing scheme to cycle the cells. The cells were discharged (lithiated) and charged (delithiated) with various cycling currents between 0.05 and 1 V (versus Li/Li^+). The conducted rate study was carried out with charging rates ranging from (*C*/20)–(5*C*). The discharge rates were started at *C*/20, increased to *C*/10, and maintained at this rate for subsequent cycling. Charging was conducted with constant current (CC) and discharge was conducted with CCCV cycling parameters.

Material Characterization: An FIB (field-emission ionization (FEI), NOVA200 dual-beam system) equipped with an air-lock chamber was used for TEM sample preparation.[10] TEM and EELS analysis was performed with an FEI Tecnai F20 operated at 200 keV. A detailed description of the TEM and EELS characterization procedures can be found elsewhere.[22]

Supporting Information

Supporting Information is available from the Wiley Online Library or from the author.

Acknowledgements

This work was supported by the Assistant Secretary for Energy Efficiency and Renewable Energy, Office of Vehicle Technologies for the U.S. Department of Energy under Contract No. DE-AC-36-08GO28308, subcontract No. NFT-8-88527-01 under the Batteries for Advanced Transportation Technologies (BATT) Program, by a grant from the Fundamental R&D Program for Technology of World Premier Materials funded by the Ministry of Knowledge Economy, Republic of Korea (10037919), and the National Science Foundation (NSF, DMR-1206462).

Received: September 19, 2013
Revised: November 4, 2013
Published online: December 18, 2013

[1] U. Kasavajjula, C. Wang, A. J. Appleby, *J. Power Sources* **2007**, *163*, 1003.
[2] J.-M. Tarascon, M. Armand, *Nature* **2001**, *414*, 359.
[3] B. A. Boukamp, G. C. Lesh, R. A. Huggins, *J. Electrochem. Soc.* **1981**, *128*, 725.
[4] P. Poizot, S. Laruelle, S. Grugeon, L. Dupont, J.-M. Tarascon, *J. Power Sources* **2001**, *235*, 97.

[5] X. H. Liu, L. Zhong, S. Huang, S. X. Mao, T. Zhu, J. Y. Huang, *ACS Nano* **2011**, *6*, 1522.
[6] L. A. Riley, A. S. Cavanagh, S. M. George, Y. S. Jung, Y. Yan, S.-H. Lee, A. C. Dillon, *ChemPhysChem* **2010**, *11*, 2124.
[7] M. Gu, Y. Li, X. Li, S. Hu, X. Zhang, W. Xu, S. Thevuthasan, D. R. Baer, J.-G. Zhang, J. Liu, C. Wang, *ACS Nano* **2012**, *6*, 8439.
[8] A. Magasinki, P. Dixon, B. Hertzberg, A. Kvit, J. Ayala, G. Yushin, *Nat. Mater.* **2010**, *9*, 353.
[9] C. K. Chan, H. L. Peng, G. Liu, K. McIlwrath, X. F. Zhang, R. A. Huggins, Y. Cui, *Nat. Nanotechnol.* **2008**, *3*, 31.
[10] S.-B. Son, S. C. Kim, C. S. Kang, T. A. Yersak, Y.-C. Kim, C.-G. Lee, S.-H. Moon, J. S. Cho, J.-T. Moon, K. H. Oh, S.-H. Lee, *Adv. Energy Mater.* **2012**, *2*, 1226.
[11] a) J. Saint, M. Morcrette, D. Larcher, L. Laffont, S. Beattie, J.-P. Pérès, D. Talaga, M. Couzi, J.-M. Tarascon, *Adv. Funct. Mater.* **2007**, *17*, 1765; b) T. Zhang, L. Fu, J. Gao, L. Yang, Y. Wu, H. Wu, *Pure Appl. Chem.* **2006**, *78*, 1889.
[12] D. Molina Piper, T. A. Yersak, S.-H. Lee, *J. Electrochem. Soc.* **2013**, *160*, A77.
[13] a) D. Molina Piper, T. A. Yersak, S.-B. Son, S. C. Kim, C. S. Kang, K. H. Oh, C. Ban, A. C. Dillon, S.-H. Lee, *Adv. Energy Mater.* **2013**, *3*, 697; b) G. Liu, S. Xun, N. Vukmirovic, X. Song, P. Olalde-Velasco, H. Zheng, V. S. Battaglia, L. Wang, W. Yang, *Adv. Mater.* **2011**, *23*, 4679; c) H. Wu, G. Yu, L. Pan, N. Liu, M. T. McDowell, Z. Bao, Y. Cui, *Nat. Commun.* **2013**, *4*, 1943.
[14] J. Luo, X. Zhao, J. Wu, H. D. Jang, H. H. Kung, J. Huang, *J. Phys. Chem. Lett. 2012*, *3*, **1824**.
[15] a) I. D. Scott, Y. S. Jung, A. S. Cavanagh, Y. Yan, A. C. Dillon, S. M. George, S.-H. Lee, *Nano Lett.* **2010**, *11*, 414; b) Y. S. Jung, A. S. Cavanagh, L. A. Riley, S. H. Kang, A. C. Dillon, M. D. Groner, S. M. George, S.-H. Lee, *Adv. Mater.* **2010**, *22*, 2172; c) L. A. Riley, S. Van Atta, A. S. Cavanagh, Y. Yan, S. M. George, P. Liu, A. C. Dillon, S.-H. Lee, *J. Power Sources* **2011**, *196*, 3317; d) X. Meng, X. Q. Yang, X. Sun, *Adv. Mater.* **2012**, *24*, 3589; e) Y. S. Jung, A. S. Cavanagh, A. C. Dillon, M. D. Groner, S. M. George, S. H. Lee, *J. Electrochem. Soc.* **2010**, *157*, A75.
[16] A. Dameron, D. Seghete, B. B. Burton, S. D. Davidson, A. S. Cavanagh, J. A. Bertrand, S. M. George, *Chem. Mater.* **2008**, *20*, 3315.
[17] R. A. Hall, Ph.D. Dissertation, University of Colorado at Boulder, July, **2013**.
[18] S. M. George, B. Yoon, A. A. Dameron, *Acc. Chem. Res.* **2009**, *42*, 498.
[19] B. H. Lee, B. Yoon, A. I. Abdulagatov, R. A. Hall, S. M. George, *Adv. Funct. Mater.* **2013**, *23*, 532.
[20] a) D. Aurbach, Y. Ein-Eli, B. Markovsky, A. Zaban, S. Luski, Y. Carmeli, H. Yamin, *J. Electrochem. Soc.* **1995**, *142*, 2882; b) K. Kanamura, H. Tamura, S. Shiraishi, Z.-I. Takehedra, *J. Electroanal. Chem.* **1995**, *394*, 49; c) E. Peled, D. Golodnitsky, G. Ardel, *J. Electrochem. Soc.* **1997**, *144*, L208.
[21] a) J. W. Wang, Y. He, F. Fan, X. H. Liu, S. Xia, Y. Liu, C. T. Harris, H. Li, J. Y. Huang, S. X. Mao, T. Zhu, *Nano Lett.* **2013**, *13*, 709; b) X. H. Liu, H. Zheng, L. Zhong, S. Huang, K. Karki, L. Q. Zhang, Y. Liu, A. Kushima, W. T. Liang, J. W. Wang, J.-H. Cho, E. Epstein, S. A. Dayeh, S. T. Picraux, T. Zhu, J. Li, J. P. Sullivan, J. Cummings, C. Wang, S. X. Mao, Z. Z. Ye, S. Zhang, J. Y. Huang, *Nano Lett.* **2011**, *11*, 3312; c) X. H. Liu, Y. Liu, A. Kushima, S. Zhang, T. Zhu, J. Li, J. Y. Huang, *Adv. Energy Mater.* **2012**, *2*, 722.
[22] S.-B. Son, J. E. Trevey, H. Roh, S.-H. Kim, K.-B. Kim, J. S. Cho, J.-T. Moon, C. M. DeLuca, K. K. Maute, M. L. Dunn, H. N. Han, K. H. Oh, S.-H. Lee, *Adv. Energy Mater.* **2011**, *1*, 1199.